Fractured Reservoir Prediction – A Case Study in the Sichuan Basin*

Ling Yun[1], Xiangyu Guo[1], Qianggong Song[1], and Weisheng He[1]

Search and Discovery Article #10512 (2013)
Posted August 26, 2013

*Adapted from extended abstract prepared in conjunction with oral presentation at AAPG Annual Convention and Exhibition, Pittsburgh, Pennsylvania, May 19-22, 2013,

[1]RGC, BGP, CNPC, Zhuozhou, Hebei, China (lingyun@bgp.com.cn)

Abstract

Fractured reservoir is one of important reservoir types for hydrocarbon exploration, and a major target for shale gas exploration. The geophysicists have presented diverse techniques for the fractured reservoir detection in the literature, such as fast and slow shear waves, azimuthal attributes of P-wave, AVOZ of P-wave and pre-stack inversion. The application of these techniques is challenging for the deep reservoir because the seismic data are usually poor caused by the problems in seismic acquisition design and processing. In this paper, the research targets at the fracture prediction in the fluvial clastic reservoir in Sichuan Basin, including the acquisition design of VSP and full-azimuth surface seismic, VSP processing and parameter estimation, VSP-driven surface seismic processing, structural and depositional interpretation, and the fracture prediction using attributes extracted from P-wave surface seismic data, VSP data and well logging data. The case study shows that diagenesis study is necessary for the fractured reservoir detection, and different methods should be applied for the reservoirs with continental and marine facies. For the reservoir with continental facies, the sedimentary facies interpretation is required to predict the fracture-developed zones in the reservoir. Based on that, the forming model of the oil and gas reservoir should be researched to predict the hydrocarbon-bearing fractured reservoir.

Introduction

Anisotropic theory was introduced to the geophysics in the late nineteenth century. Berryman (1979), Crampin (1983) and Helbig (1983, 1984) began to study the anisotropy of the thin reservoir in 1980s. Afterwards, Tsvankin (1994) and Alkhalifah (1995) presented the equation of nonhyperbolic reflection moveout in anisotropic media. Schoenberg (1995) and Bakulin (2000) proposed methods for the estimation of the fracture parameters from reflection seismic data. The theory of VTI, HTI and TTI has made great contributions to the exploration of the fractured reservoir.

Background of the Oilfield

The study area is located in Southwest China. The depth of the target clastic reservoir is greater than 4500 meters. The relief structure is about 262.5m. The porosity varies from 1.8% to 8.7%. The permeability is between 0.004×10^{-3} to $0.847\times10^{-3}\mu m^2$. There are several formations of hydrocarbon source rocks. Six wells have been drilled in the high position of the structure, and three of them with gas show, but none of industrial value. However, the data of its adjacent area show that the permeability can reach $0.1\mu m^2$ in the fracture-developed region, and the gas reservoir with high productivity was found.

Considering the characters of the low relief structure and the fractured reservoir, and the assumptions for HTI and VTI media, we first extract the earth absorption parameter, velocity model, HTI and VTI parameters from the VSP data. Second, these parameters are used to drive the surface seismic processing. Finally, the processed seismic data are used for detecting the fractures in the reservoir. So the paper covers the acquisition design for Zero-offset VSP (ZVSP), eight directional Walkaway-VSP (WVSP) and full-azimuth surface seismic data, the processing of VSP data, parameter extraction from VSP data, surface seismic processing driven by VSP data, reservoir structural and depositional interpretation, attribute extraction from surface seismic data, fracture prediction using VSP, well logging and surface seismic data.

Acquisition Design for VSP and Surface Seismic Data

According to the characters of the fractured reservoir with low relief structure and the requirement for the estimation of the earth absorption parameter and velocity in the seismic processing, ZVSP acquisition is designed to cover the depth from 200m to 5,290m with the receiver space interval of 10m and time interval of 1ms.

According to the requirement for the estimation of HTI and VTI parameters, eight directional WVSP was designed. The receivers were put in the range of 200m to 5,290m in depth. The receiver space interval is 10m and time interval is 1ms. In the study area, the structural trend varies from NE in the lower formations to NEE in the upper formations. Therefore, the azimuths of WVSP are designed as 21.312º (L1), 66.312º (L2), 111.312º (L3) and 156.312º (L4). The maximum offset is 4.7km. The source interval is 100m.

In order to predict the fracture reservoir, the full-azimuth of the surfaces seismic observation is designed (Aspect ratio 1:1, Receiver lines 32, Max offset 9000m, Max fold 128, Bin size 25m×25m). The inline direction is the same as L1 of WVSP, 21.312º. The acquisition design of VSP and 3D surface seismic is shown in Figure 1.

Parameter Estimation from VSP Data and VSP-Driven Surface Seismic Processing

ZVSP processing and parameter estimation. The processing flow for ZVSP and WVSP data is shown in Figure 2. In this workflow, we focus on estimating the parameters for wave propagation in the subsurface and the validation of these parameters to drive the WVSP and the surface seismic data processing. Two procedures in ZVSP processing workflow are different from the conventional workflow. One is the way to estimate the T- and Q-compensation factors with scanning approach. The other is that deconvolution parameter is calculated from up-going

wave instead of down-going wave. These parameters are more conductive to drive the WVSP and surfaces seismic processing than conventional method.

Figure 3 and 3b show the raw ZVSP data and their corresponding amplitude spectrum. After ZVSP processing, we get the T- and Q-compensation factors. T factor is 2.4. Q factor is 10 at 0ms, 10 at 1,000ms, 20 at 1,400ms, 25 at 1,700, 30 at 2,000ms, 40 at 2,300ms and 50 at 6,000ms respectively.

The ZVSP image and amplitude spectrum after processing are shown in Figure 4a and 4b, respectively. Comparing Figure 4 with Figure 3, we can see that the energy of the data is well compensated and the frequency bandwidth is broadened from 10-40Hz to 10-125Hz after processing.

In addition, the ZVSP velocity is approximately equivalent to the average velocity at normal incidence and it can be used to convert to the interval velocity and RMS velocity. It differs from the velocity obtained from surface seismic data. It is also different from the well logging velocity that has more components of high frequency. The VSP data is almost equal to the smoothed well logging velocity, which can be seen in Figure 5a. Using the ZVSP velocity can help to convert the seismic data from time to depth or depth to time. Figure 5b shows that the ZVSP data matches the surface seismic data very well.

ZVSP-driven WVSP processing. The WVSP data is acquired in the more similar way with the surface seismic data than the ZVSP data in terms of the source-receiver offset. Therefore, the WVSP velocity should be more close to the surface seismic velocity, and the velocity field of WVSP can be used for surface seismic processing. Moreover, the receiver point of the ZVSP is the same as the WVSP's. Therefore, we can combine ZVSP and WVSP data to estimate the HTI and VTI parameters. The eight directional WVSP data is very important for the estimating the anisotropic parameters and driving the surface seismic processing.

The WVSP processing flow driven by ZVSP data is shown in Figure 2. T-compensation factor, Q-compensation factor, deconvolution operator and velocity at normal incidence obtained from ZVSP data are used for WVSP processing. The result of WVSP before and after processing is shown in Figure 6. Comparing Figure 6a and 6b, we can find that the energy attenuation due to the earth absorption is well compensated. Figure 6c shows that the bandwidth is broadened from 12-40Hz to 10-70Hz after processing. In addition, Figure 6d indicates that the wavelet becomes more stable after processing.

The travel time of P-wave, which is different from true travel time observed in WVSP data, can be calculated using the velocity of ZVSP and forward modeling with the isotropic assumption (Figure 7a). The time difference, which indicates that the media is actually not isotropic, is shown in Figure7c and 7d. Base on it, travel time is calculated with the VTI media (Figure 7b) assumption, and then VTI parameter at well location can be estimated by fitting the time difference with least square method (Figure 7d). Figure 7d shows that the theory of VTI media is favorable to the true media than the isotopic media. Therefore, the processing image of WVSP and surface seismic data that is driven by the VTI parameter and velocity of ZVSP should be better than the isotropic assumption.

In the same way, the each direction of VTI parameters are calculated with the eight directions of WVSP data, and shown in Figure 8. Based on it, HTI parameter for all depths can be calculated by the oval HTI theory and shown in Figure 9b. Of course, the HTI parameters of the fracture

reservoir at 4,500m shown in Figure 9c can be obtained and used to predict the direction and size of the fractures, to calibrate and interpret the result of the surface seismic distribution.

VSP-driven surface seismic processing. Figure 10 shows the processing and quality control flow for surface seismic processing driven by T- and Q-compensation factors, deconvolution operator, velocity at normal incidence, VTI and HTI parameters obtained from the VSP and WVSP data. In the processing flow, T- and Q-compensation factors and deconvolution operators are used to compensate the amplitude attenuation for surface seismic data. The comparisons of ZVSP data to surface seismic data before and after compensation processing are shown in Figure 11a and 11b respectively. The corresponding amplitude spectra are shown in Figure 11c and 11d, which indicates the energy of surface seismic data is well compensated with the introduced workflow.

The source energy of surface seismic data varies spatially due to the surface condition or other factors. The change in source energy caused by these factors should be considered in the processing. The spatial variation of the source energy is shown in Figure 12a, and four raw shot gathers in Figure 12a, which is used for quality control of surface seismic processing. The result after processing is shown in Figure 13. Comparing Figure 13a to Figure 12a, we can see that the special variation of the source energy is almost compensated after processing. The same phenomena can be seen by comparing Figure 12b to Figure 13b.

Afterwards, NMO velocity can be obtain via velocity analysis according to the criterion of flattening the reflections. The velocity spectrum, picked NMO velocity and flattened CMP gathers are shown in Figure 14a at well position. If using of ZVSP's velocity for the conventional NMO correction, the same CMP gathers would look like overcorrected in Figure 14b, which implies that the ZVSP velocity is not suitable for surface seismic data with the isotropic assumption. Therefore, with the ZVSP velocity, VTI parameter and appropriate equation of VTI's NMO correction, the reflections in Figure 14c become flattened. In this way, the seismic image can be certainly improved. AVO analysis, prestack inversion and predicting the fractured reservoir are more reliable.

Fracture Prediction Using P-Wave Seismic Data

Structural and depositional interpretation. For predicting the fractured reservoir, the methods of fracture detection are mostly concerned and the importance of geological interpretation is relatively ignored. However, we consider that the structural and depositional interpretation for the fractured reservoir is compulsory like the case study for the conventional reservoirs. The reason is that the proper prediction method can be chosen only if the structure and sedimentary facies is correctly interpreted.

With the help of the well logging, ZVSP and WVSP data for seismic horizon calibration, two seismic horizons are picked up. Two profiles along the yellow lines in the base map are shown in Figure 15a and 15c, and two structural maps of these two horizons are shown in Figure 15b and 15d respectively. The six wells are mainly located in the high position. However, no commercial gas or oil is found because the fractures are not well developed at well locations. After structural interpretation, the depositional interpretation is believed to be essential although the sand in the reservoir is very tight. The purpose of depositional interpretation is to characterize the changes in the rock property.

By the well logging data (Figure 16a), the deposition environment of delta front in the reservoir can be obtained. Based on it, the channel deposition can be obtained by the interpretation of the seismic RMS amplitude extracted along the reservoir layers shown in Figure 16b and the profile shown in Figure 16c. The blue dash lines in Figure 16d, which are along low amplitude, are interpreted as four fluvial channels that come from two directions. One of them comes from south. The others come from northeast.

Fracture prediction using VSP-driven surface seismic data. It seems that there is no relationship between the structural or depositional interpretation and the fracture detection. However, the shale content in the rock has an impact on the way and the degree of the rock rupture under the same stress. We assume that the fluvial deposition makes the variation in shale content, which makes the fracture developing inhomogeneous in the subsurface under the same stress.

Based on this assumption, we firstly extract the curvature attribute from surface seismic data along the reservoir layer (Figure 17a). The curvature attribute interpretation of good fracture zones that are shown with dotted polygons indicates 90 percent of them located at the fluvial channels from RMS amplitude in Figure 17b. Secondly, both the frequencies and phases of the seismic wave are changing when it propagates in the HTI media. Therefore, the frequency and phase attributes, which are shown in Figure 17c and 17d, are not stable in the area with fluvial channels. The above analysis of the relationship between the seismic attributes (curvature, frequency, phase and RMS amplitude) and sedimentary facies indicates that the fracture developing in the reservoir is related to sedimentary facies, shale content and stress field. Finally, the image logging data are shown in Figure 18a and indicate that the fractures are mainly in east-west direction. This coincides with the direction of the fractures predicted from WVSP data (Figure 9). The study shows that the stress field is mainly in south-north direction. Combining all of these results and the sedimentary facies interpreted from seismic attributes, we consider that the fracture developing and structure deformation can easily happen inside the fluvial channel under the same stress field (Figure 18c). In addition, an azimuth angle gather where fractures exist is shown in Figure 18d. In Figure18d, the travel time (yellow line) varies with the azimuth angle. According to the theory for wave propagation in the HTI media that the travel time is shortest along the direction of the fracture, we also know that the fracture is manly in east-west direction in Figure 18d. Overall, we believe that the direction of fractures is mainly east-west. Using the fractures predicted from all available data, some new wells are suggested. The logging data of new wells prove that the predicted fracture distribution is reliable.

Conclusions

The following conclusions have been drawn though the application to an oilfield in Sichuan Basin:

(1) Using proper seismic acquisition techniques are very important for successful prediction of the fractures in the reservoir.
(2) VSP data can provide the parameters for the wave propagation in the earth, especially velocity at normal incidence, VTI and HTI parameter. These parameters can drive the surface seismic processing. In addition, HTI and VTI parameters can be used for predicting the fractures that is valuable information for calibrating the fracture result predicted from the surface seismic data.
(3) The introduced full-azimuth seismic processing flow driven by VSP data can give reliable seismic data for the fracture prediction.
(4) The structural and depositional interpretation is essential for the fracture prediction in the clastic reservoir.
(5) The fracture-developed zones can be predicted using the seismic attributes, well logging data, stress field and genesis of fractured reservoir.

References Cited

Alkhalifah, T., and I. Tsvankin, 1995, Velocity analysis for transversely isotropic media: Geophysics, v. 60/5, p. 1550–1566.

Bakulin, A., V. Grechkaz, and I. Tsvankinz, 2000, Estimation of fracture parameters from reflection seismic data—Part I: HTI model due to a single fracture set: Geophysics, v. 65/6, p. 1788-1802.

Berryman, J.G., 1979, Long wave elastic anisotropy in transversely isotropic media: Geophysics, v. 44/5, p. 896-917.

Crampin, S., 1983, Shear-wave polarizations: A plea for three-component recording: 53rd Annual International Meeting, SEG, Expanded Abstracts, p. 425–428.

Helbig, K., 1983, Elliptical anisotropy–Its significance and meaning: Geophysics, v. 48/7, p. 825–832.

Helbig, K., 1984, Anisotropy and dispersion in periodically layered media: Geophysics, v. 49/4, p. 364-373.

Schoenberg, M. and C.M. Sayers, 1995, Seismic anisotropy of fractured rock: Geophysics, v. 60/1, p. 204-211.

Tsvankin, I., and L. Thomsen, 1994, Nonhyperbolic reflection moveout in anisotropic media: Geophysics, v. 59, 1290–1304.

Tsvankin, I., 2005, Seismic Signatures and Analysis of Reflection Data in Anisotropic Media: Pergamon, Amsterdam, The Netherlands, 436 p.

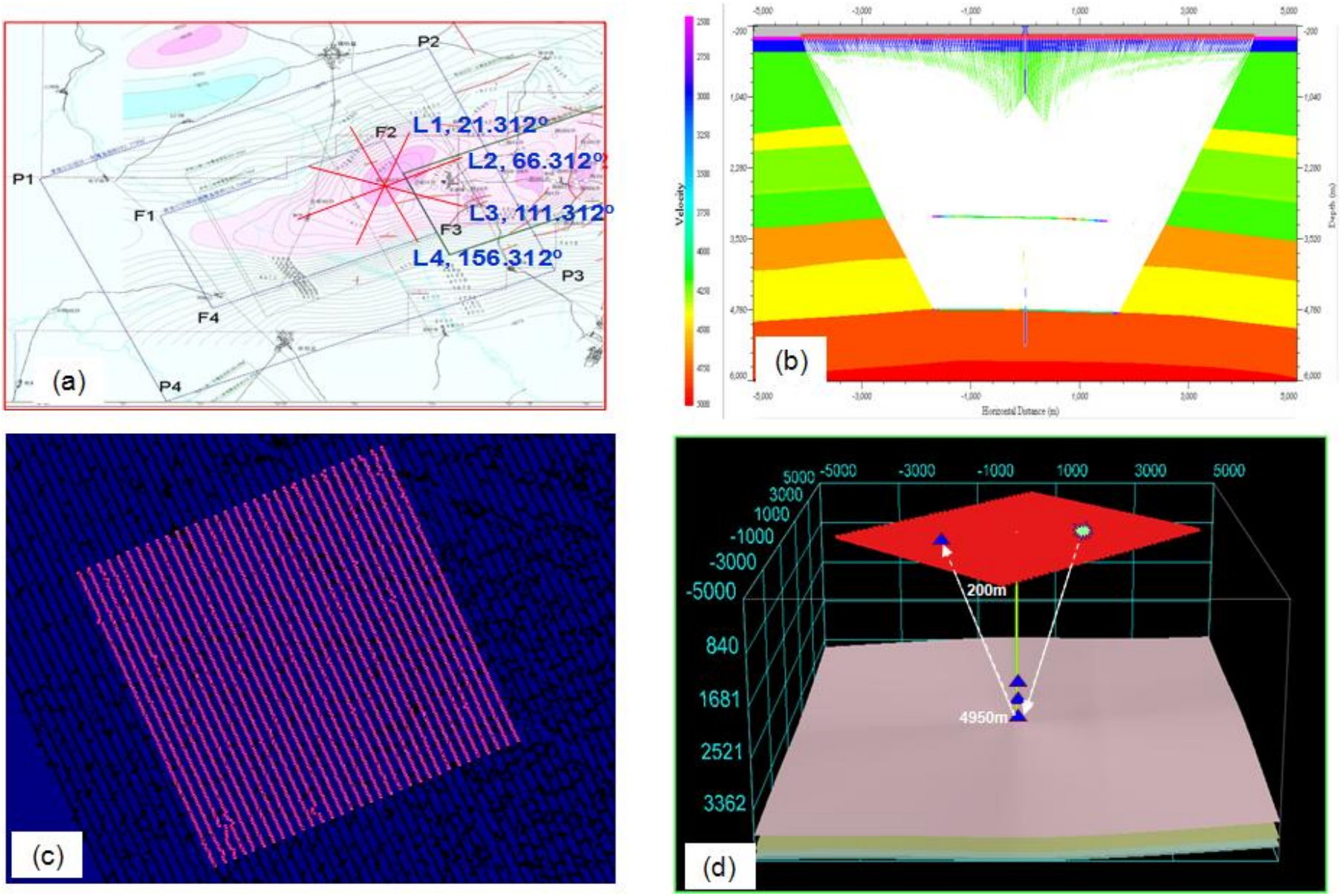

Figure 1. (a) The study area and the receiver line of WVSP. (b) Velocity model and seismic forward modeling for WVSP. (c) Surface seismic geometry. (d) The diagram of VSP and surface seismic data.

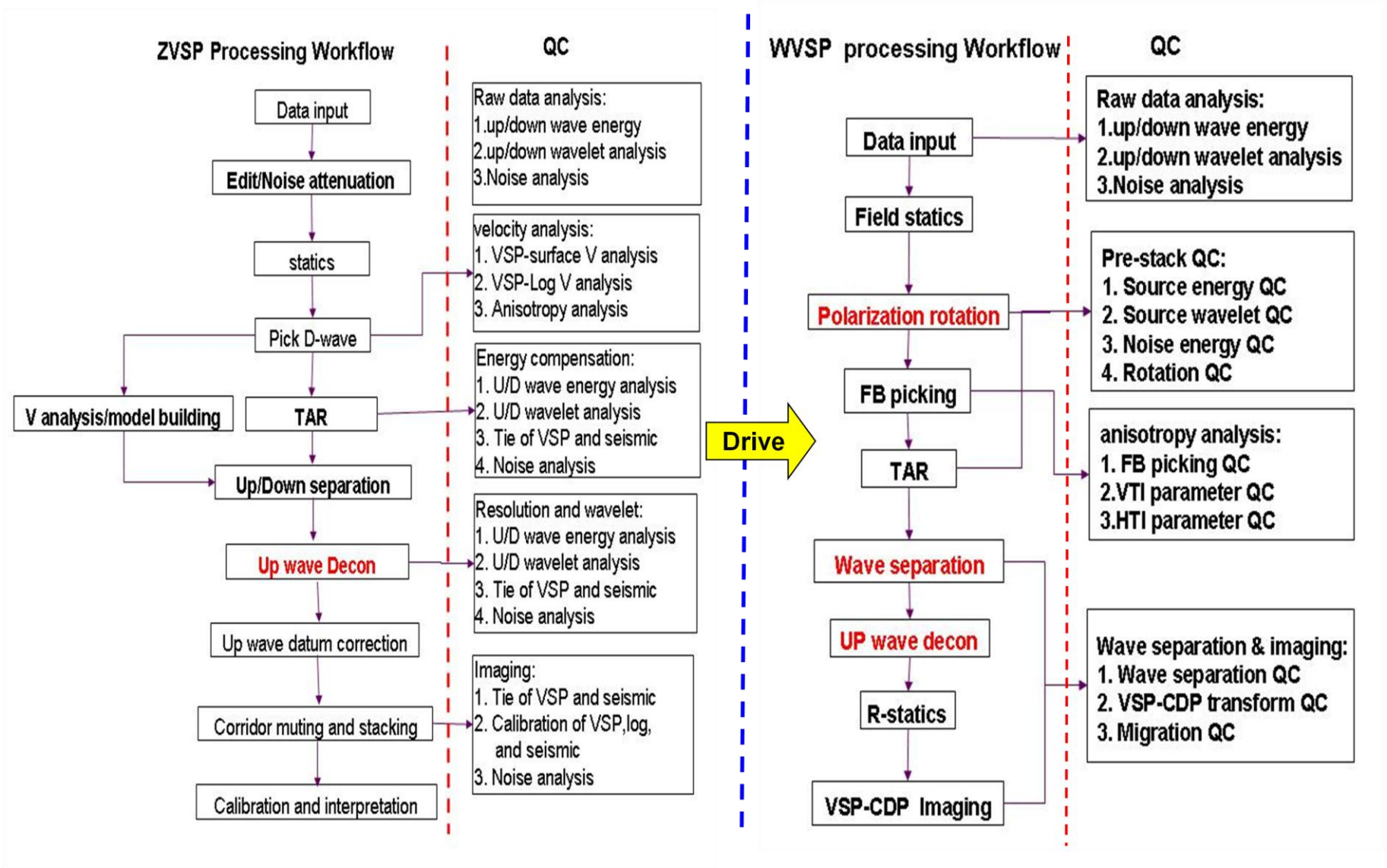

Figure 2. WVSP processing flow (right) driven by ZVSP (left).

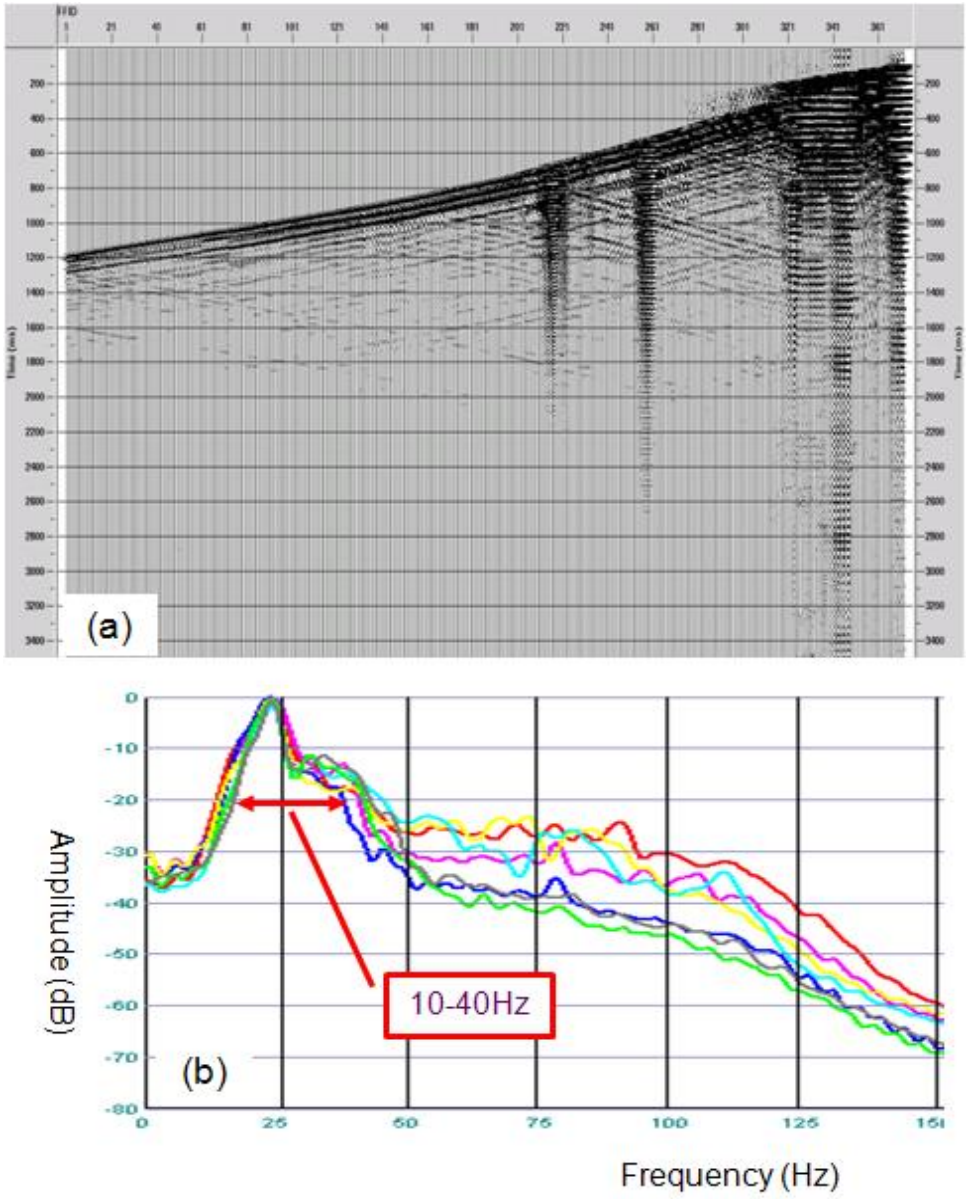

Figure 3. (a) Profile of raw ZVSP data. (b) Amplitude spectrum of (a).

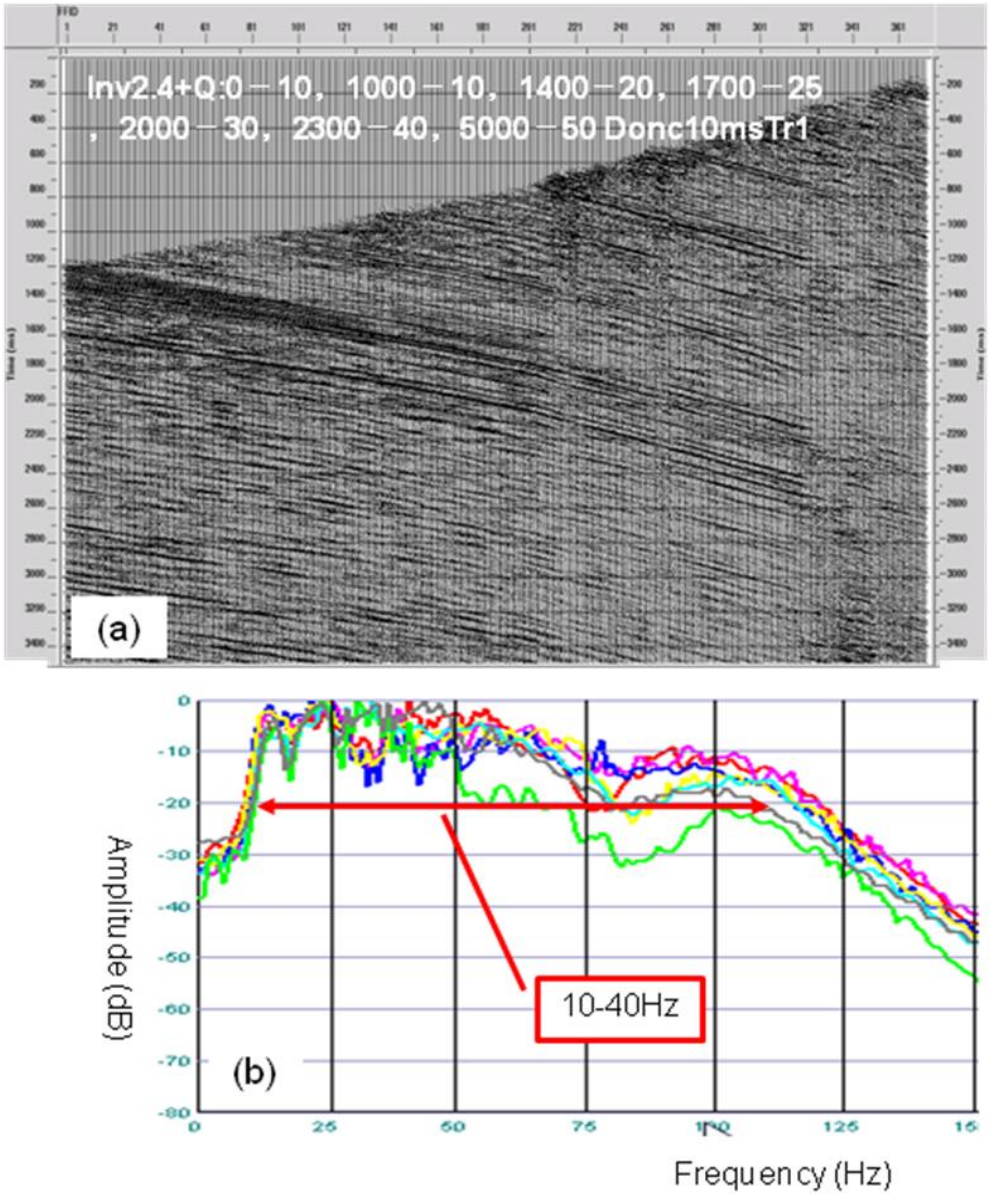

Figure 4. (a) Profile of Raw ZVSP data after processing. (b) Amplitude spectrum of (a).

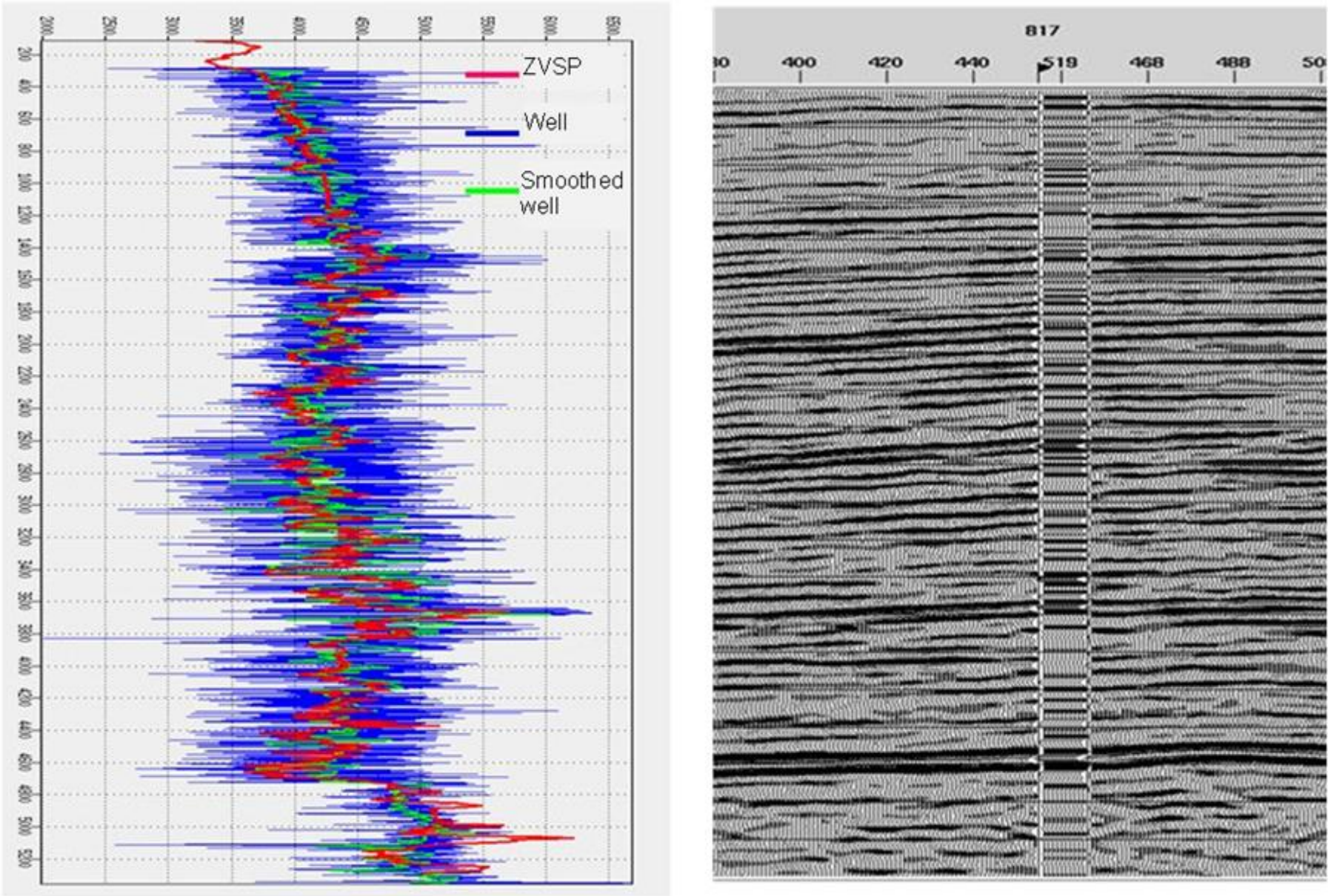

Figure 5. (a) The velocity comparison of ZVSP, well logging and smoothed well logging. (b) ZVSP data embedded (middle) in the surface seismic data (both sides).

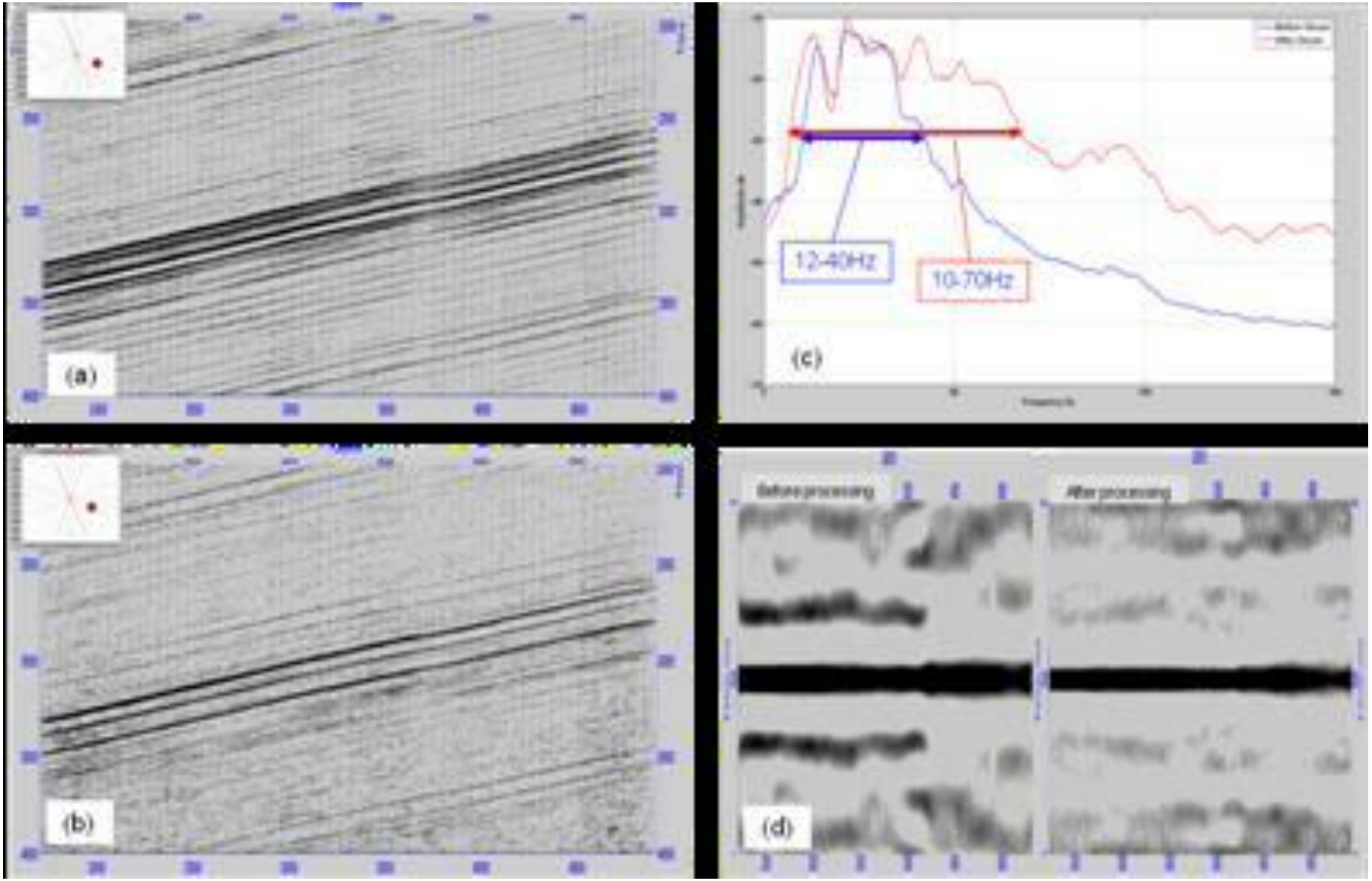

Figure 6. (a) The input WVSP image. (b) WVSP image processed with ZVSP-driven workflow. (c) The comparison of amplitude spectrum of WVSP data before processing to that after processing. (d) Wavelet comparison before (left) and after processing (right).

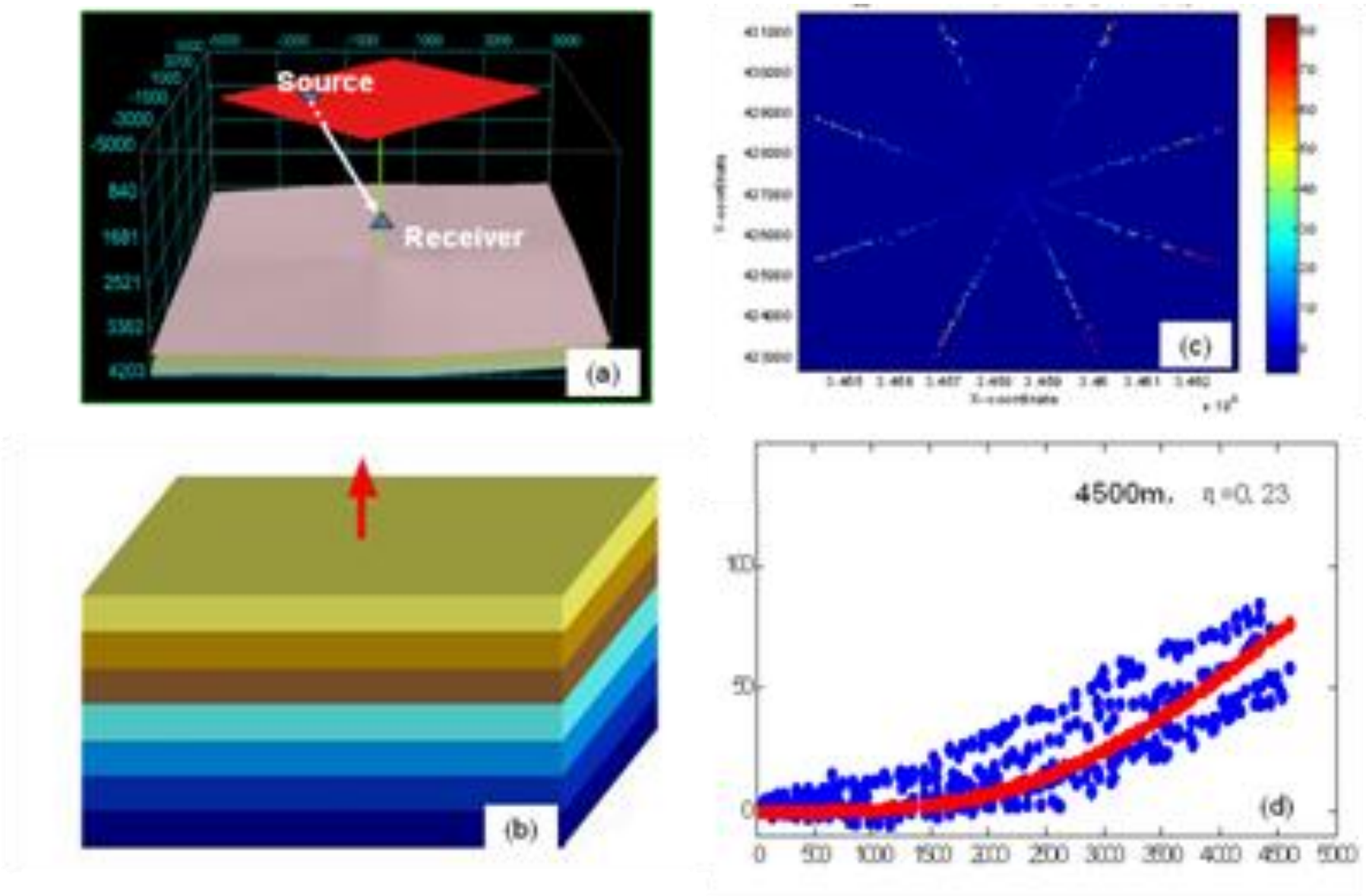

Figure 7. (a) The diagram for travel time calculation under isotropic assumption. (b) The diagram for VTI media. (c) The time difference between calculated and actual travel time. (d) The time difference and its fitting curve.

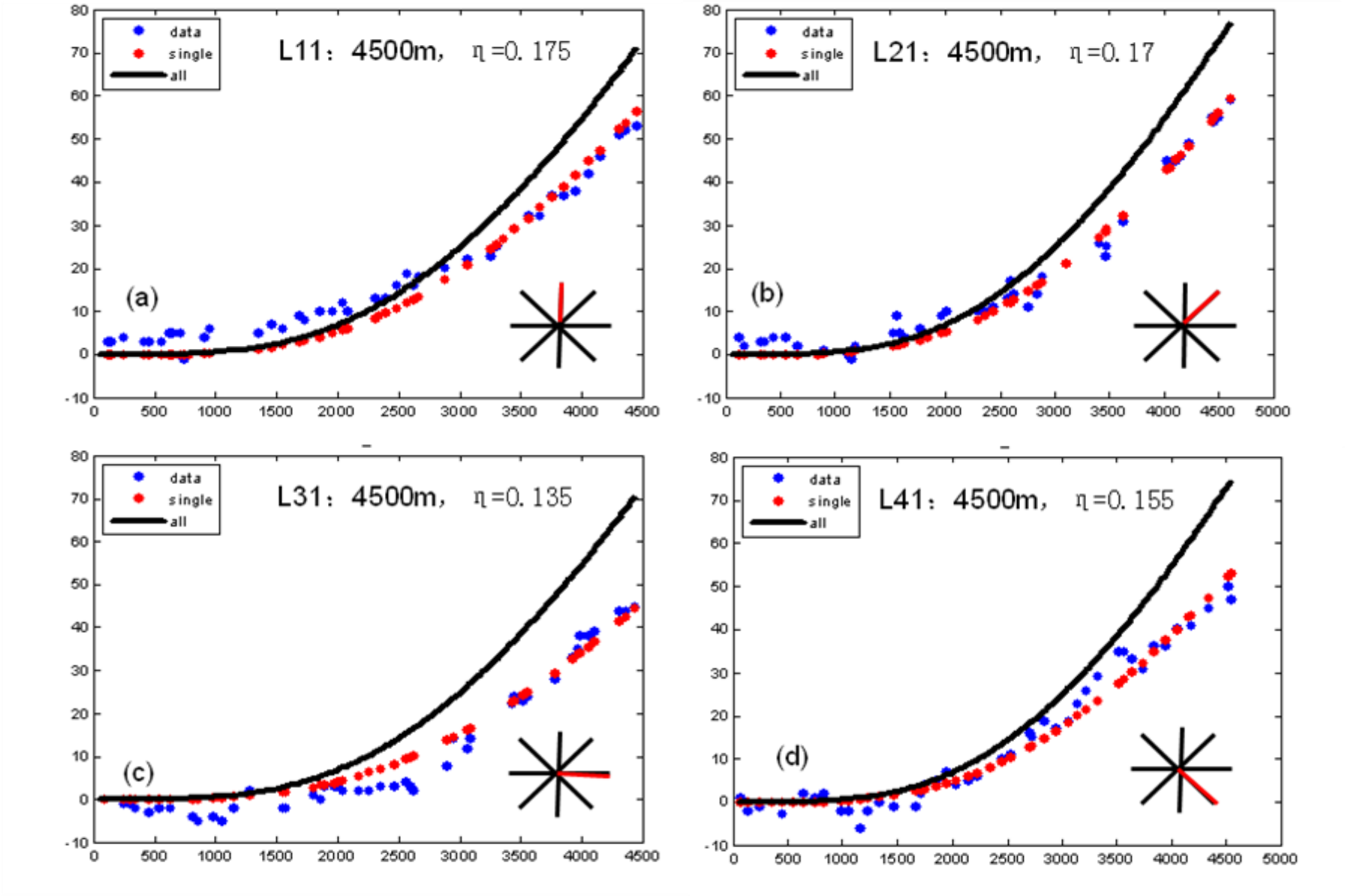

Figure 8. Travel time differences and their fitting curves for eight directions that are shown with red lines at lower-left corner of all figures.

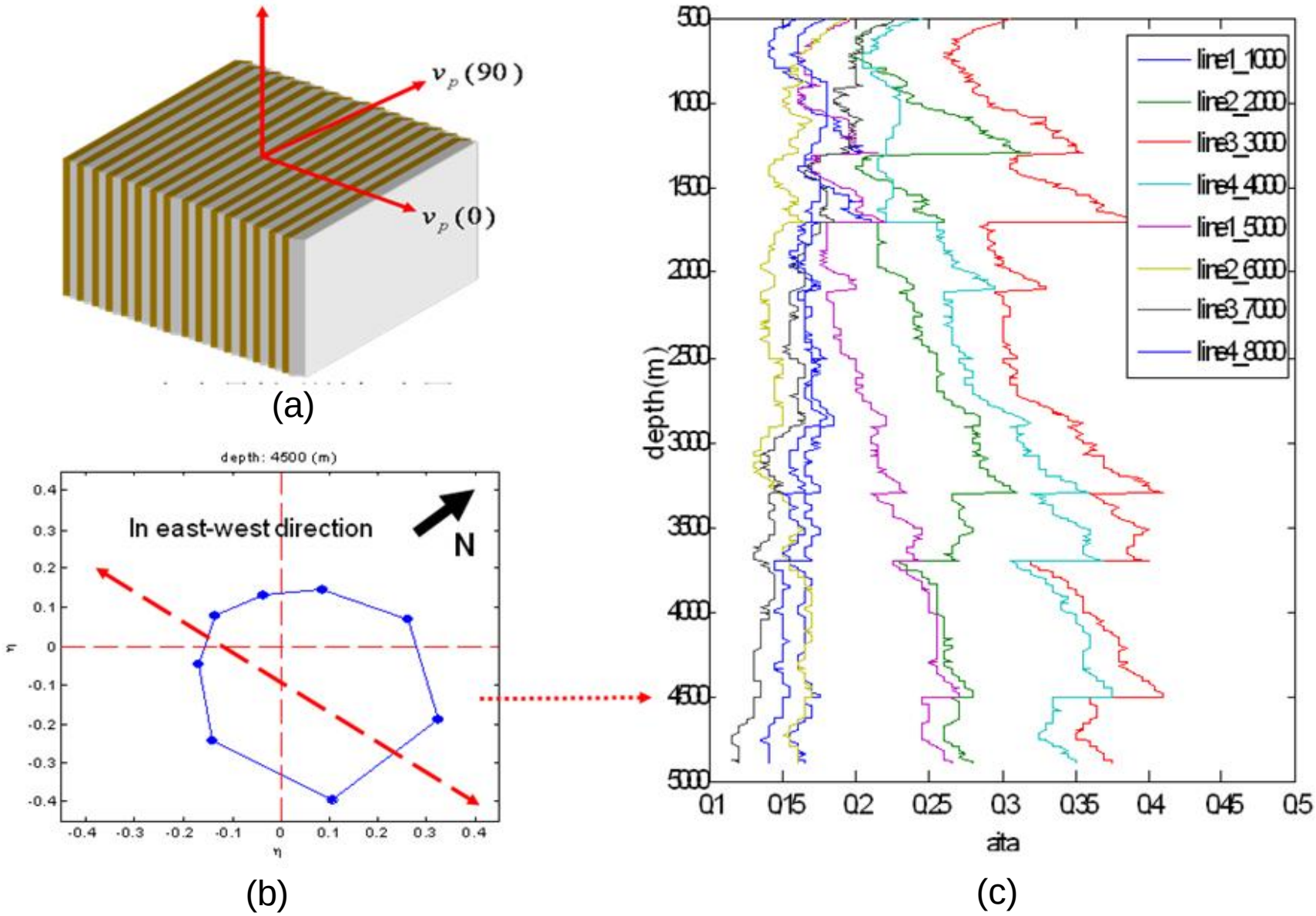

Figure 9. (a) The diagram for HTI media. (b) The HTI curves vs. depth in eight directions. (c) HTI parameters in eight directions at the fracture reservoir (4,500m).

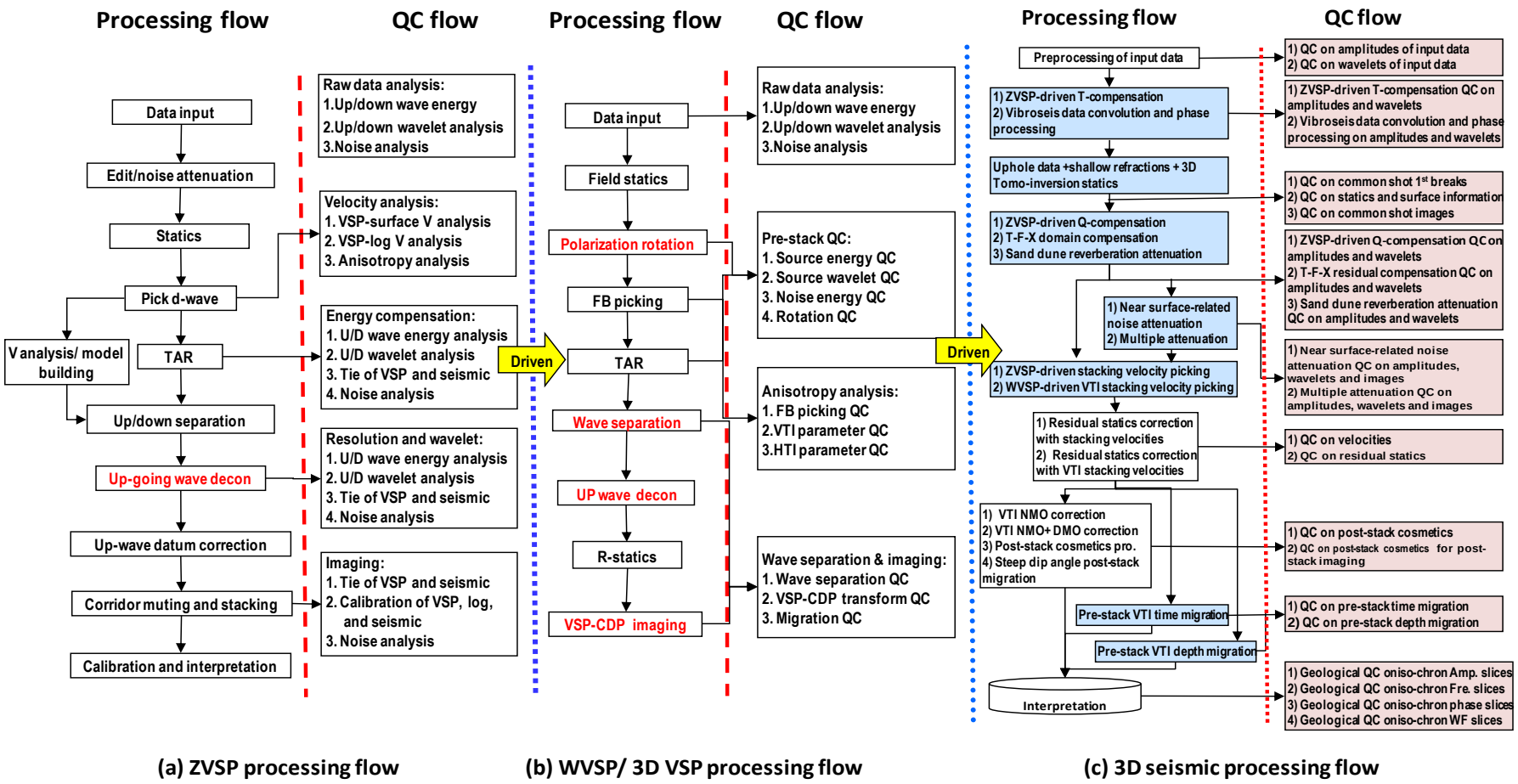

Figure 10. The workflow for seismic processing driven by ZVSP, WVSP data.

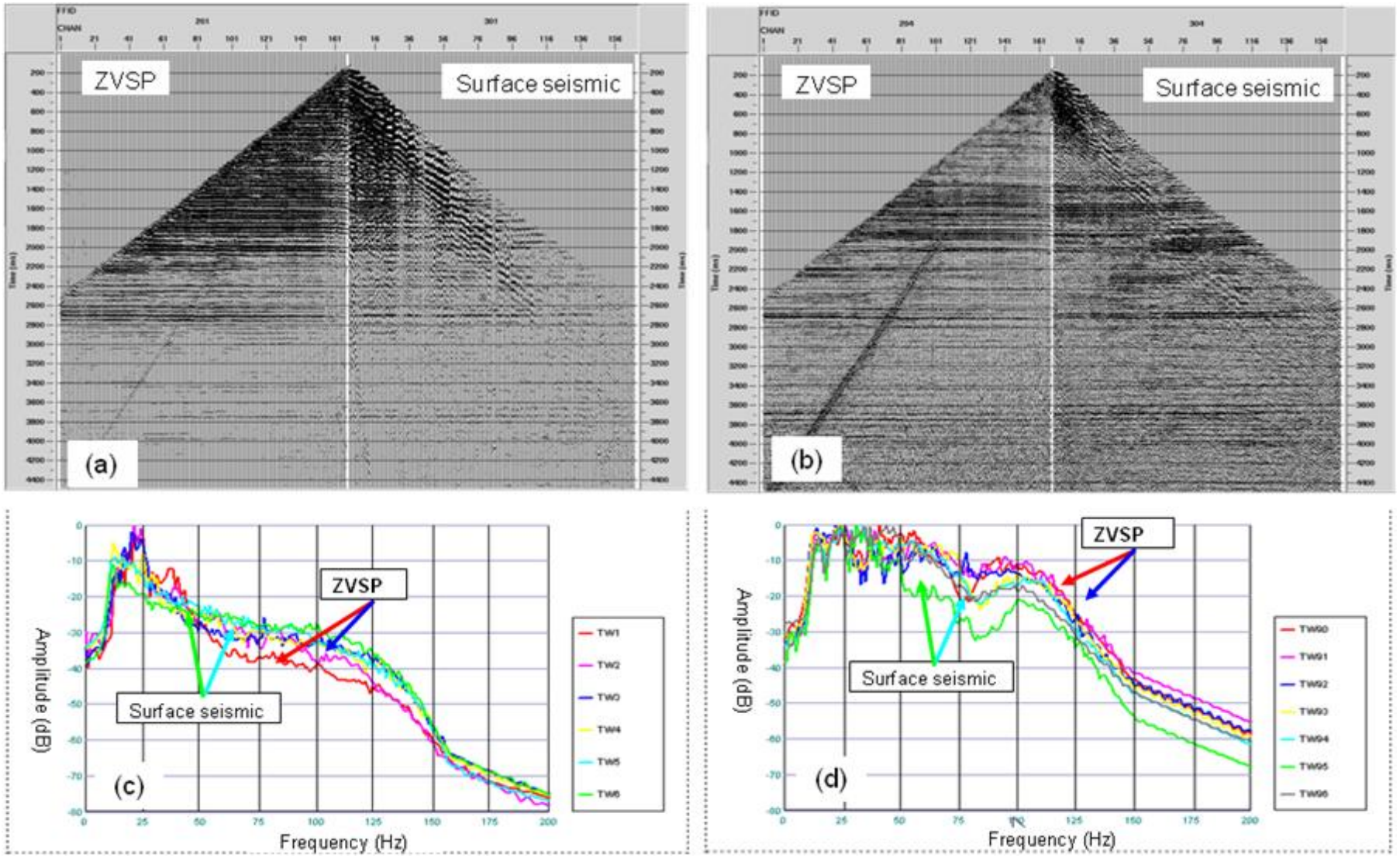

Figure 11. The comparisons of ZVSP data to surface seismic data before (a) and after compensation and deconvolution (b). Their corresponding amplitude spectra are shown in the lower figures.

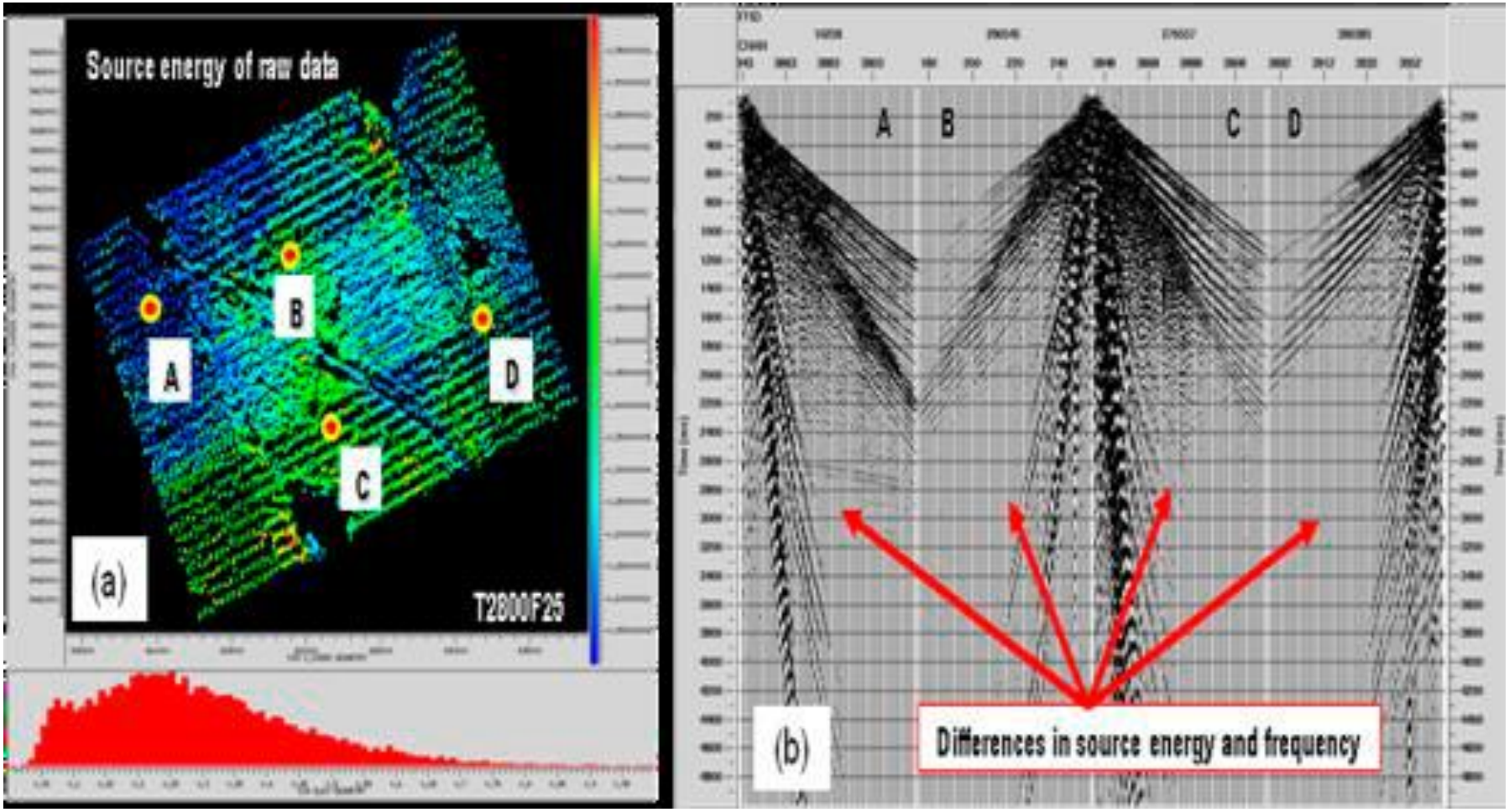

Figure 12. (a) Source energy map before T-F compensation and source deconvolution. (b) Four shot gathers with location marked in the left map.

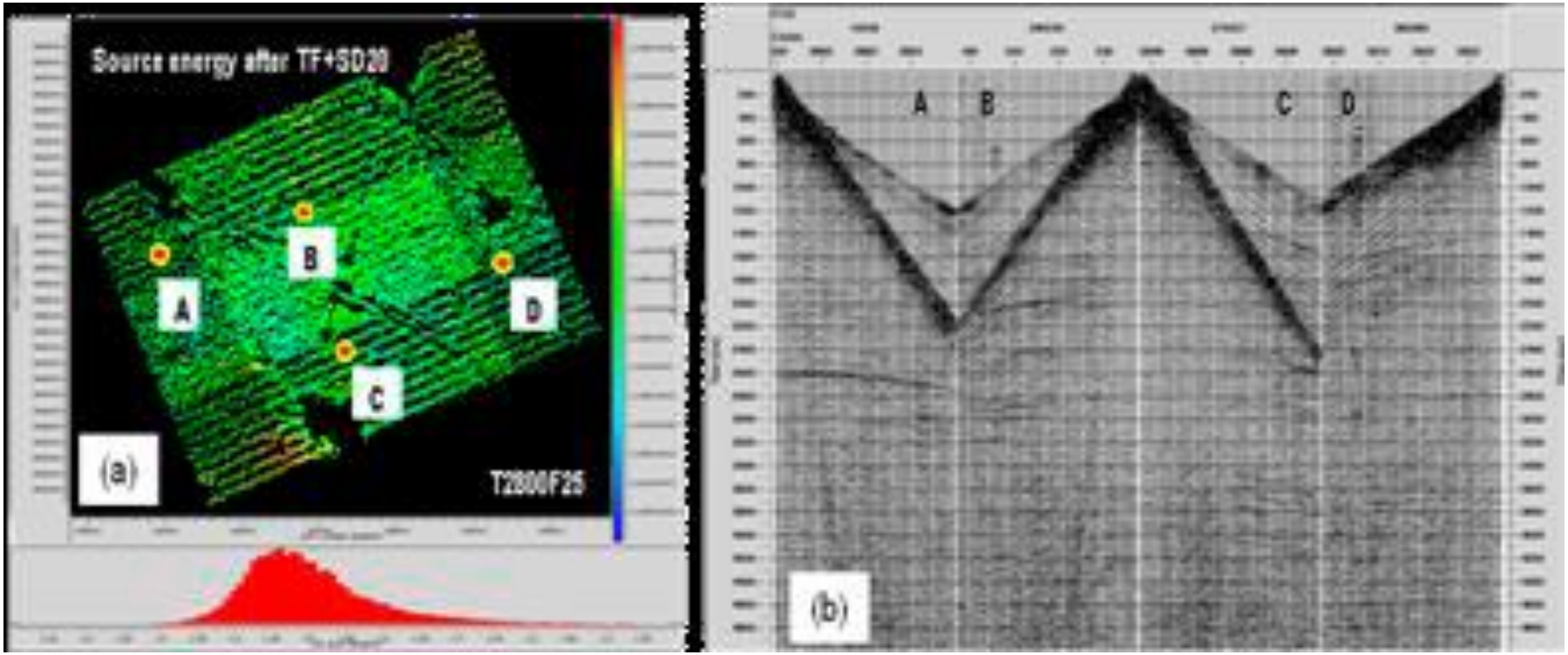

Figure 13. (a) Source energy map after T-F compensation and source deconvolution. (b) Four shot gathers located in the left map.

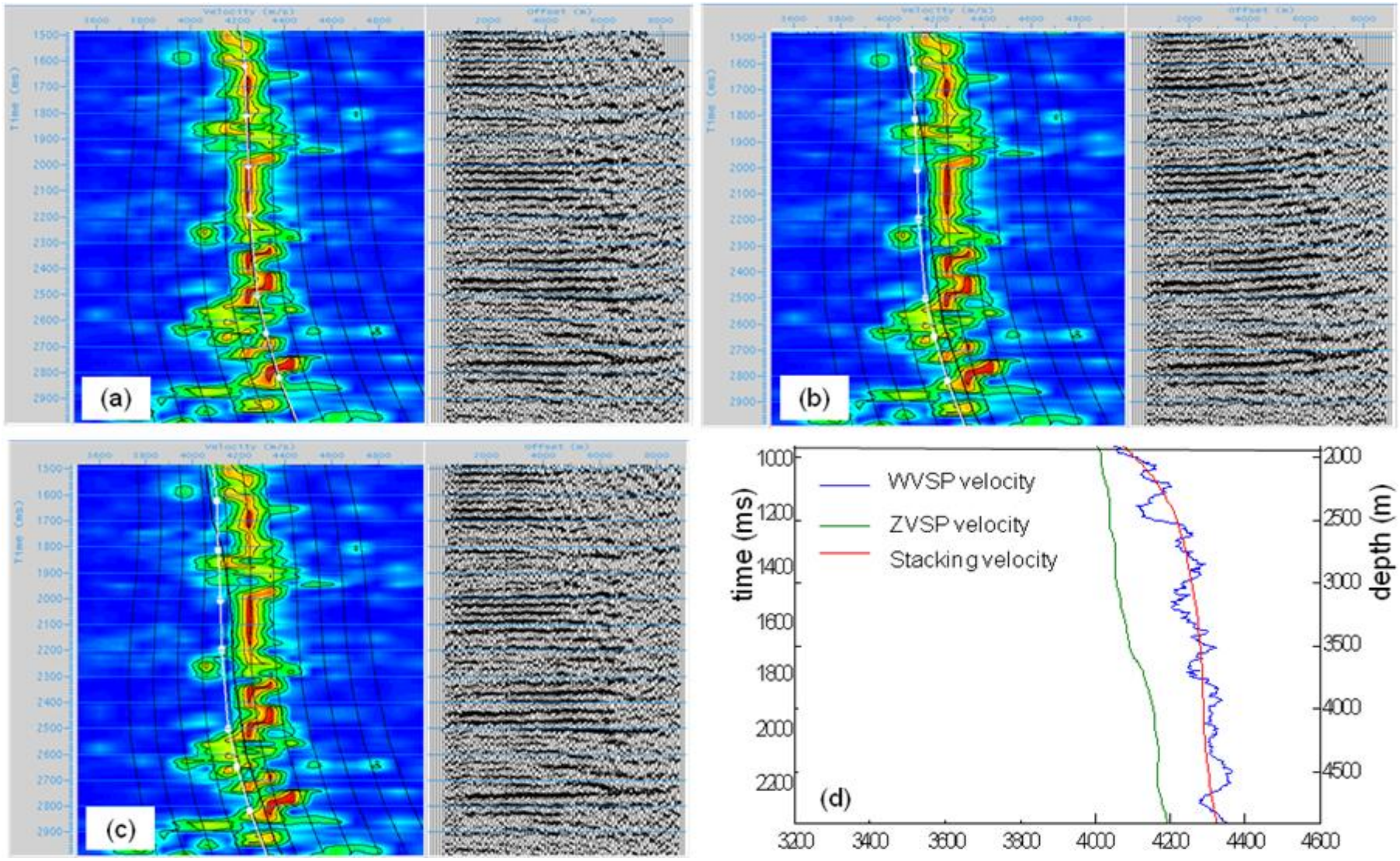

Figure 14. The comparisons of the results after NMO correction using different velocities. (a) Stacking velocity and profile after NMO correction with it. (b) ZVSP velocity and profile after NMO correction with it. (c) ZVSP velocity and profile after NMO correction with it, VTI and HTI parameter. (d) The comparison of stacking velocity, ZVSP velocity and WVSP velocity.

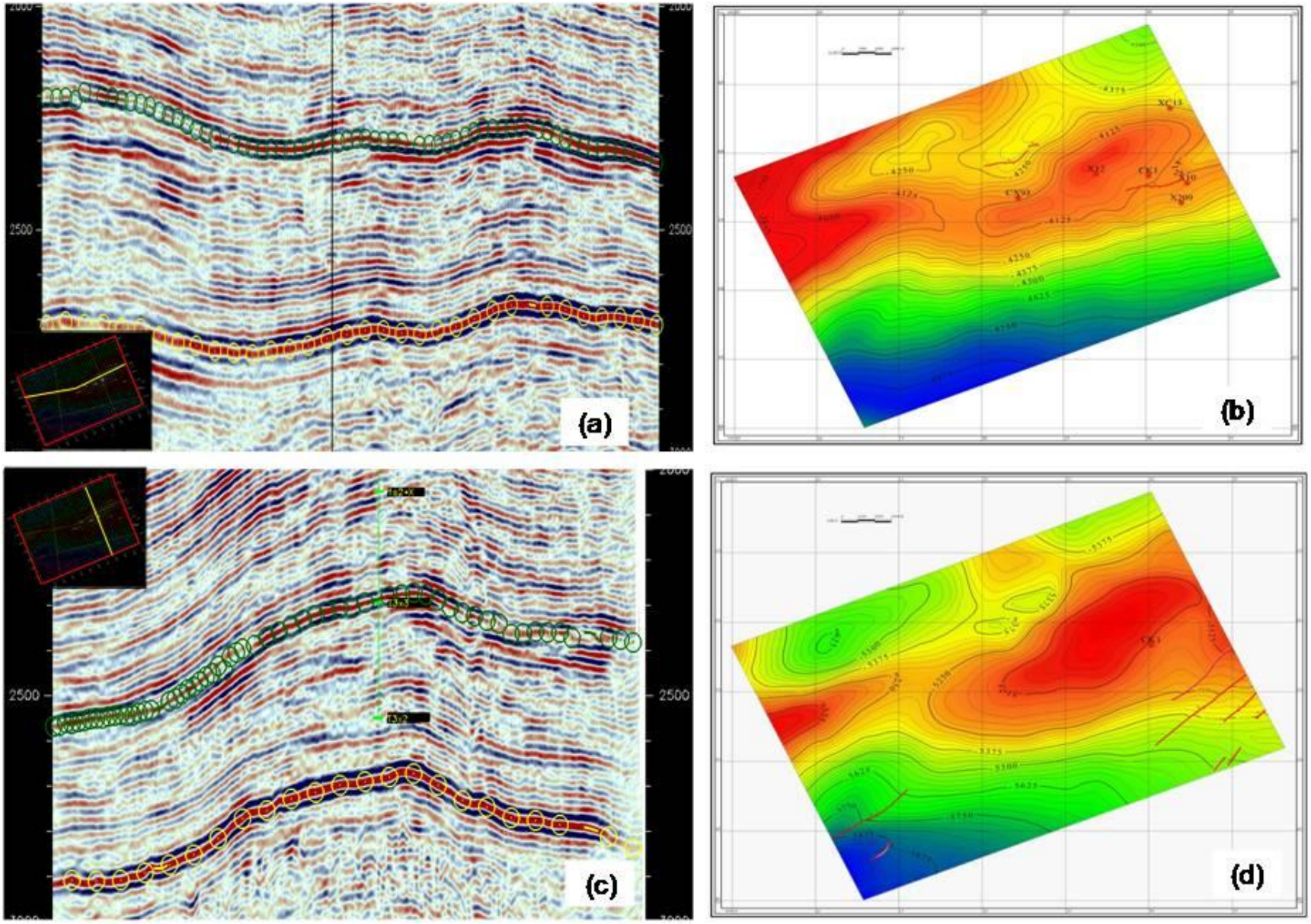

Figure 15. The seismic horizons of the top and bottom of the reservoir. (a) The seismic horizons shown on crossline profile. (b) The structure map of the top of the reservoir. (c) The seismic horizons shown on inline profile. (d) The structure map of the bottom of the reservoir.

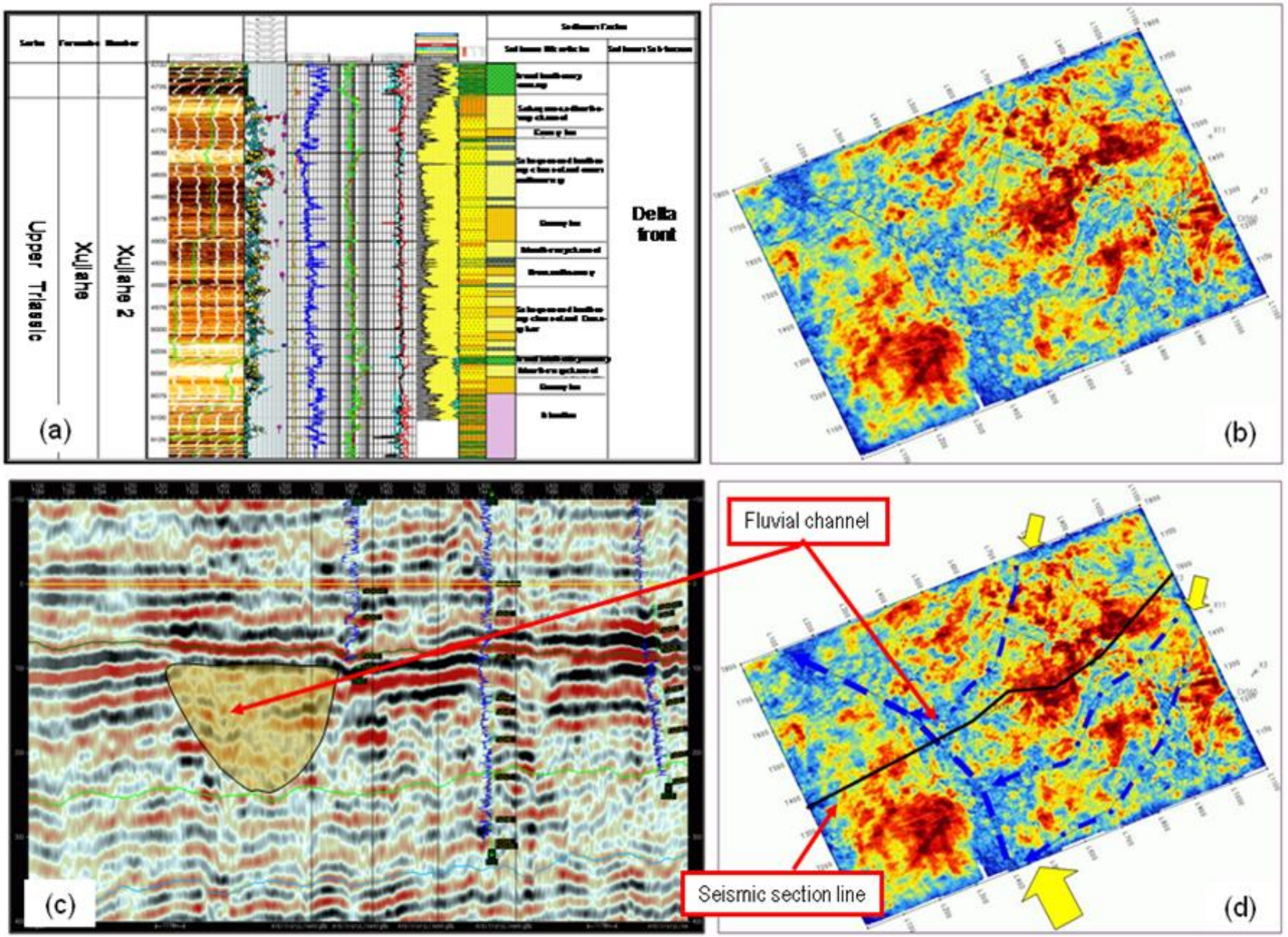

Figure 16. Sedimentary facies interpretation using well logging data and surface seismic data. (a) Sedimentary facies interpretation using well data. (b) RMS amplitude along a horizon in the reservoir. (c) Facies interpretation in seismic profile. (d) RMS amplitude along a horizon in the reservoir and facies interpretation.

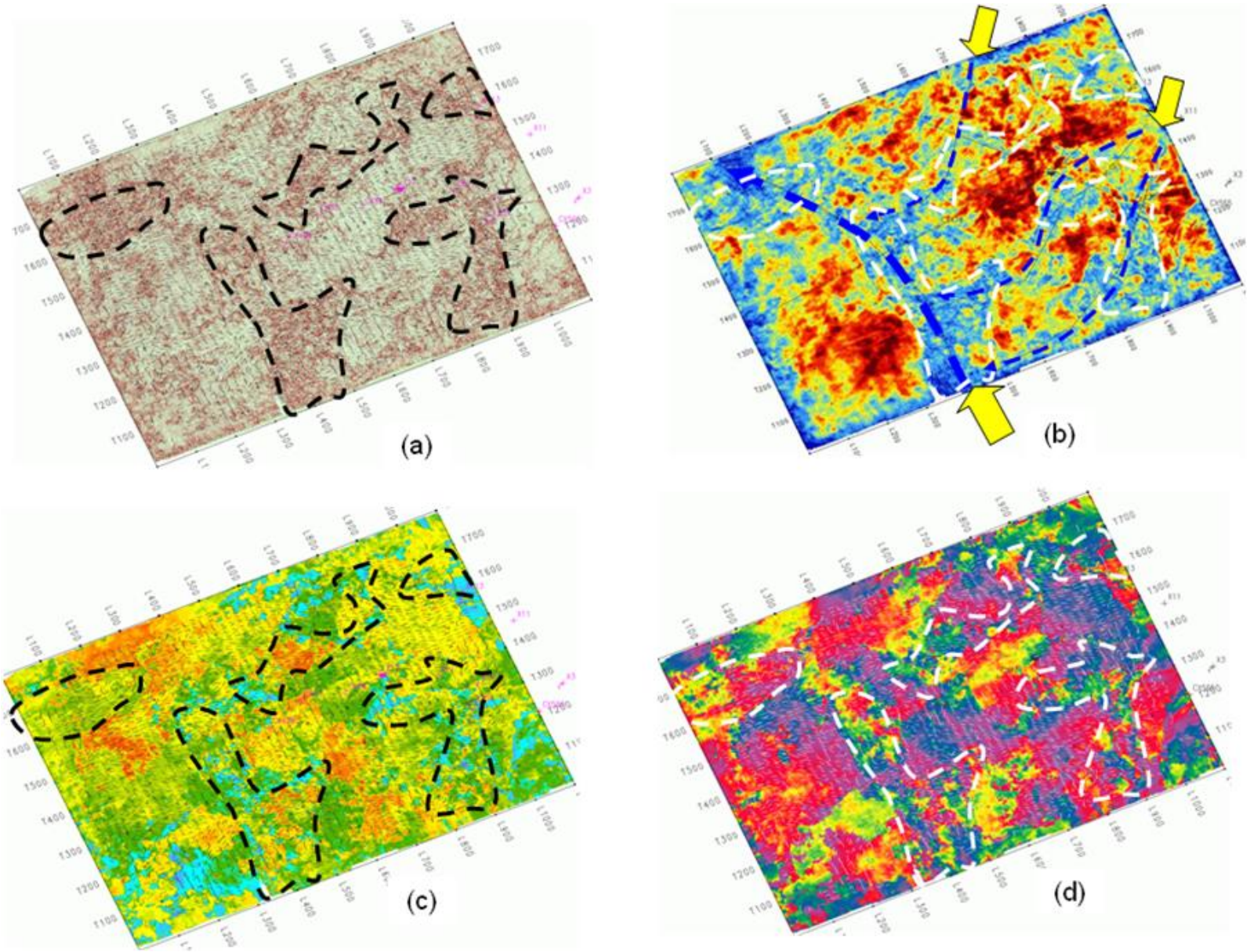

Figure 17. Fracture prediction using different seismic attributes. (a) Curvature map overlapped with fluvial channels shown with dotted polygon and the fracture map predicted from surface seismic data. (b) RMS amplitude map. (c) Frequency map. (d) Phase map.

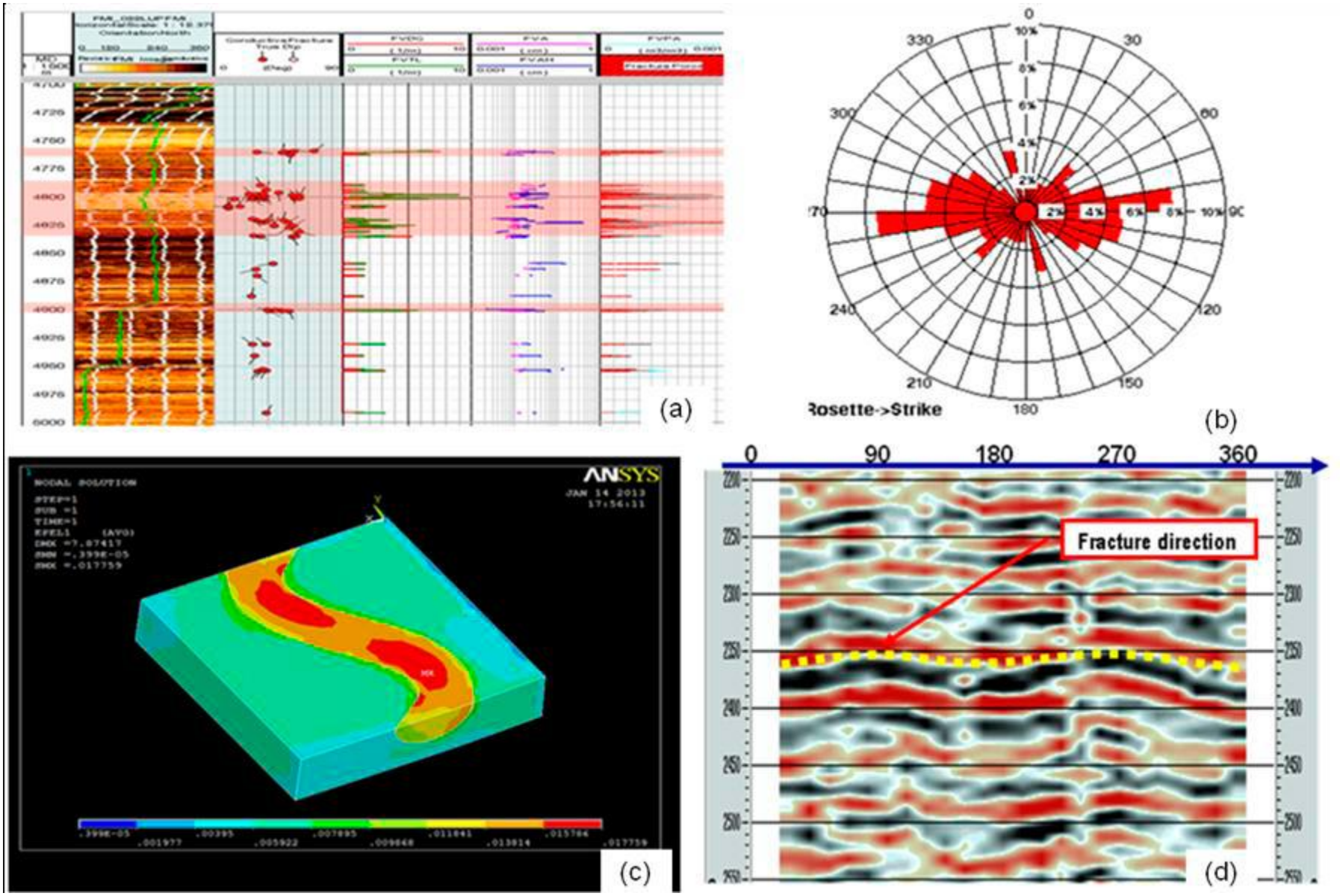

Figure 18. The analysis of the direction of the fractures using imaging well logging data (a and b) and seismic data (d). Fracture developing model under the same stress field is shown in Figure (c). The fractures can be more easily developed inside the fluvial channel than its surrounding rock under the same stress field.